Working Together: The Combined Application of a Magnetic Field and Penetratin for the Delivery of Magnetic Nanoparticles to Cells in 3D

Hannah W. Child,[†] Pablo A. del Pino,[‡] Jesus M. De La Fuente,[‡] Andrew S. Hursthouse,[§] David Stirling,[§] Margaret Mullen,[⊥] Gordon M. McPhee,[†] Colin Nixon,[∥] Vineetha Jayawarna,[#] and Catherine C. Berry[†,*]

[†]Centre for Cell Engineering, Glasgow University, Joseph Black Building, G12 8QQ, U.K., [‡]Aragon Institute of Nanoscience, Zaragoza, Spain, [§]School of Science, University of the West of Scotland, Paisley, PA1 2BE, U.K., [⊥]Integrated Microscopy Facility, Glasgow University, Joseph Black Building, G12 8QQ, U.K., [∥]The Beatson Institute for Cancer Research, Bearsden, Glasgow, G61 1BD, U.K., and [#]Department of Pure and Applied Chemistry, University of Strathclyde, Glasgow, G1 1XL, U.K.

ABSTRACT Nanoparticles (NPs) are currently being developed as vehicles for *in vivo* drug delivery. Two of the biggest barriers facing this therapy are the site-specific targeting and consequent cellular uptake of drug-loaded NPs[1]. *In vitro* studies in 2D cell cultures have shown that an external magnetic field (MF) and functionalization with cell-penetrating peptides (CPPs) have the capacity to overcome these barriers. This study aimed to investigate if the potential of these techniques, which has been reported in 2D, can be successfully applied to cells growing in a 3D environment. As such, this study provides a more realistic assessment of how these techniques might perform in future clinical settings. The effect of a MF and/or penetratin attachment on the uptake of 100 and 200 nm fluorescent iron oxide magnetic NPs (mNPs) into a fibroblast-seeded 3D collagen gel was quantified by inductively coupled plasma mass spectrometry. The most suitable mNP species was further investigated by fluorescence microscopy, histology, confocal microscopy, and TEM. Results show that gel mNP uptake occurred on average twice as fast in the presence of a MF and up to three times faster with penetratin attachment. In addition, a MF increased the distance of mNP travel through the gel, while penetratin increased mNP cell localization. This work is one of the first to demonstrate that MFs and CPPs can be effectively translated for use in 3D systems and, if applied together, will make excellent partners to achieve therapeutic drug delivery *in vivo*.

KEYWORDS: magnetic nanoparticles · cell-penetrating peptides · magnetic field · 3D culture · collagen gel · cellular uptake

Disease treatments, such as chemotherapy, currently lack specificity,[1,2] thus cytotoxicity is a common problem, as the drugs administered attack both healthy and diseased cells alike. It is hoped that nanoparticles (NPs) can be used to solve this problem by carrying and delivering drugs specifically into diseased cells, thereby preventing the attack of healthy cells and improving drug efficacy.[3,4] In addition, it is anticipated that NP-mediated delivery of nucleic acids will enable the long-awaited clinical use of gene therapy.[5] Two of the biggest problems currently facing NP-mediated drug delivery are the site-specific targeting and subsequent cellular uptake of NPs within the body (*e.g.*, into cancerous cells within a tumor).

One favorable method to improve NP targeting is to distally control their movement within the body through the application of an external magnetic field (MF).[6] Magnetic NPs (mNPs) such as those composed of iron oxide are ideal for use in this targeting strategy since they display good biocompatibility,[7−9] strong magnetism,[10] useful imaging properties (such as MRI),[11,12] and ease of functionalization and have been extensively researched *in vitro*.[13] The effectiveness of magnetic targeting of mNPs has already been exemplified *in vitro* by its widescale use as a research tool for gene transfection, this popular technique being coined "magnetofection".[14−18] In light of the efficiency of magnetic NP targeting already seen *in vitro* it is hoped that a MF can be used in the same way *in vivo* to successfully target magnetic NPs to the site of disease within the human body.

Once at the site of disease, NPs face the second problem of cellular uptake, an essential feat required for delivery of their therapeutic payload. NP functionalization with cell penetrating peptides (CPPs) is a promising solution to this hurdle.[19] CPPs such as Tat and penetratin are short, highly basic, peptide sequences (<20 amino acids) known to promote cargo transport across the plasma membrane.[20,21] Their ability to promote cellular uptake of NPs was first reported in 1999, when Josephson *et al.* demonstrated a 100-fold increase in Tat-functionalized NP uptake.[22] Since then, increased cellular uptake of NPs functionalized with CPPs has been

* Address correspondence to Catherine.berry@glasgow.ac.uk.

Received for review June 13, 2011 and accepted September 6, 2011.

Published online September 06, 2011
10.1021/nn202163v

repeated in numerous *in vitro* studies.[23−27] However, despite such encouraging findings, CPPs are not receptor-dependent and, thus, not cell-specific.[28−30] Therefore, to enable site-specific drug delivery, they will need to be used in conjunction with a targeting strategy, such as a MF.

This study has investigated the combined use of a 280 mT MF with a CPP (penetratin) in order to simultaneously improve both targeting and uptake of mNPs to human fibroblasts. The novelty of this study lies in the use of a 3D tissue-equivalent model where cells are cultured within a type-1 collagen gel matrix.[31,32] The use of this 3D model provides a cell culture environment that is more comparable to *in vivo* tissue than are traditional 2D monolayer cultures. This is important, since research in 2D monolayer cell cultures may not reliably predict later-stage clinical responses to therapeutic NPs.[33−35] This is because in the latter scenario cells are surrounded by and interact with the extracellular matrix (ECM), which can produce phenotypic differences, altering behavior to that observed in monolayer cell culture.[36,37] Therefore 2D testing of NP delivery systems is ultimately of limited use, as NP behavior may be very different once introduced into a living system. In response to this problem, this 3D study provides a more accurate prediction of how a MF and penetratin could be used to deliver drug-loaded mNPs to diseased cells inside the human body.

Results demonstrate that while a MF increases the rate and depth of mNP uptake into the gel, penetratin encourages cell−NP association and subsequent cellular uptake. Thus a combination of both would be recommended for therapeutic drug delivery *in vivo*. This study represents an important stepping-stone in the journey from traditional 2D research toward the development of a NP-based drug delivery system for clinical use.

RESULTS

NP Characterization. TEM allowed visualization of the four mNP species (Figure 1). The sizes of the mNPs are described as 100 and 200 nm by Chemicell. However, in TEM both species appear much smaller, as only the electron-dense core is visible. Since the aggregation seen here could have been caused by the TEM processing, additional characterization was performed using a Malvern Zetasizer (Suppoprting Information, Table 1). Analysis of particle size by dynamic light scattering confirmed that the 100 nm species are not aggregated, but that the 200 nm species are slightly aggregated into groups of 5−10 particles. In addition, an increase in particle negativity as measured by zeta potential confirmed the successful attachment of penetratin (Suppoprting Information, Table 1).

Gel Characterization. *Rheology and Atomic Force Microscopy (AFM).* The Young's modulus (stiffness) of the gel was found to be 2 ± 1.7 kPa (mean ± SD) as measured by AFM, being comparable to the Young's modulus of human fibroblast cells, which is reported as 2−60 kPa, as measured by AFM.[38] Rheology is a method of measuring a material's elasticity (termed elastic modulus) through the application of force. In this case, the elastic modulus of the gel was found to be between 1 and 10 kPa (Figure 2) as measured by rheology, being comparable to the elastic modulus of human adipose tissue as tested by rheology (3−6 kPa).[39] The AFM and rheology results presented here both demonstrate that the gels have a consistency similar to human tissue, highlighting the suitability of this cell culture model for use in realistic 3D studies.

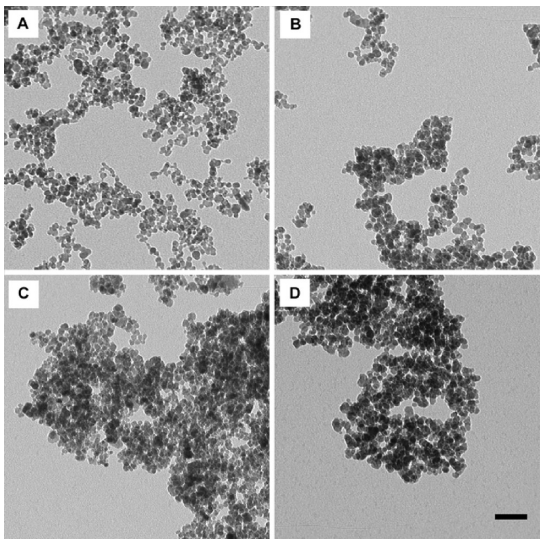

Figure 1. TEM images of the four mNP species. Images represent plain 100 nm mNPs (A), 100 nm with penetratin (B), plain 200 nm mNPs (C), and 200 nm with penetratin (D). Note that the polysaccharide matrix, the fluorescent dye, and the penetratin peptide (16 amino acids) surrounding the mNPs cannot be seen by TEM. Hence this figure shows only the electron-dense iron core of each mNP [scale bar = 50 nm].

Microscopy Characterization. Gels were further analyzed to determine cell distribution and viability in the 3D construct (Figure 3). SEM images show cells growing in a confluent, parallel sheet over the top surface of the gel (Figure 3A) with collagen fibers visible between the cells (Figure 3B). These fibers appeared as a dense, random network with pores of less than 5 μm in diameter. The cellular extensions appear to be interacting with the collagen, becoming entwined in the fibrous network. Histology cross sections show cells distributed uniformly throughout the gel (Figure 3C and D). The surface sheet of cells as was noted in the SEM is again observable here, running along the top edge of the section (indicated by black arrows). The MSB stain shows that the collagen is fibrous in appearance and homogeneous throughout the gel (Figure 3D). The gel thus structurally presents as a dense, tissue-equivalent model.

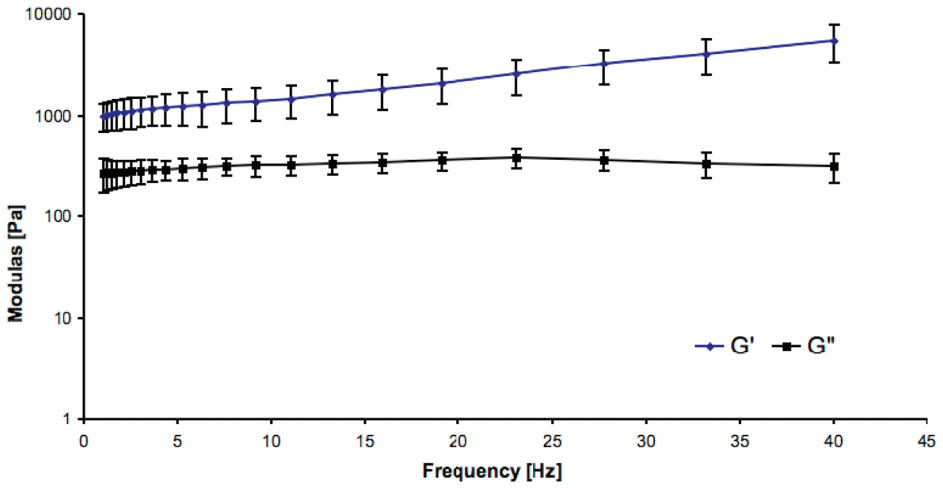

Figure 2. Gel stiffness. Graph indicates the elastic modulus (G') and the viscous modulus (G'') of the gel as measured by rheology. This figure shows that G' lies between 1 and 10 kPa, a stiffness in line with human tissue.

Live/dead staining shows cells are viable both in the center and at the edge of the gel after 96 h of culture (Figure 3E and F, respectively). No dead cells were observed. A higher density of cells is visible at the gel periphery due to gel contraction condensing this area. Cellular F-actin immunofluorescence shows a dense concentration of cells growing in a parallel fashion on the gel surface (Figure 3G), which is in agreement with SEM and histological analysis. Cells at the edge of the gel can be seen growing in line with the contour of the gel (Figure 3H).

Uptake Analysis. *Histology.* An initial qualitative assessment of mNP–gel interaction was obtained by staining histology cross sections of the gel (1 cm length $\times$ 0.5 cm width, cut to a thickness of 4 μm) with Perls Prussian blue to visualize the iron in the mNPs. All four mNP species (100 nm plain/penetratin, 200 nm plain/penetratin) were investigated, $\pm$MF, for 18 h. No differences were observed $\pm$ MF, thus only $+$MF was depicted in Figure 4. Results demonstrate that all four mNP species can become associated with the gel, being seen as dark blue/black clusters (Figure 4). Since individual mNPs are not visible at this low magnification, assessment of total uptake level is not possible. However, this figure does clearly show that groups of mNPs are abundantly present on the gel suface (upward-pointing arrows). These surface particles may be either particles interacting with cells on the top layer of the gel or perhaps larger aggregates that remain attached to the gel surface, being too large to fit between the collagen fibers. In addition, clusters of both 100 nm plain and 100 nm penetratin mNPs were noted inside the gel (downward-pointing arrows) (Figure 4), demonstrating that gel penetration has occurred. After this initial proof of gel–mNP association, more quantitative techniques were employed to assess the effect of a MF and penetratin on gel–mNP uptake.

Inductively Coupled Plasma Mass Spectrometry (ICP-MS). The amount of gel–mNP uptake was quantified by ICP-MS analysis of iron after each of the four mNP species (100 nm plain/penetratin, 200 nm plain/penetratin) had been incubated with the gel, $\pm$ a MF, for either 1 or 18 h (Figure 5). The term "uptake" is used to describe any mNP association with the gel that was not removed by washing (penetratin NPs, being positively charged, naturally repel positively charged collagen; thus no cross association was assumed). After 1 h, uptake of 100 nm mNPs was dramatically increased on average 103% by a MF ($p < 0.01$) and 162% by penetratin ($p < 0.001$), and similarly uptake of 200 nm mNPs was increased on average 103% by a MF (no significance) and 243% by penetratin ($p < 0.01$). Interestingly, at 18 h, uptake levels were comparable, irrespective of a MF or penetratin (with the exception of 200 nm penetratin without MF). Combining both a MF and penetratin simultaneously had a slightly attenuating effect on uptake of 100 nm mNPs after 1 h. After 18 h, no significant attenuating effect was seen for either size.

It is apparent from these results that the application of a MF and the presence of penetratin both increase the speed of gel–mNP uptake, with penetratin being the fastest. It is interesting to compare the effect of a MF between plain and penetratin mNPs. To do this, we take plain mNPs without a MF as the base rate of standard, "unaided" mNP–gel uptake. The data show that a MF is required to increase plain mNP uptake, whereas when penetratin is attached, this requirement no longer exists: penetratin mNPs are able to reach the maximal level of uptake after 1 h without a MF. There is little to no difference between the uptake levels induced by a MF and by penetratin. A MF has no additional effect on the level of penetratin mNP–gel uptake. Since results were similar for both sizes of mNPs, and a smaller size is deemed optimal for dense

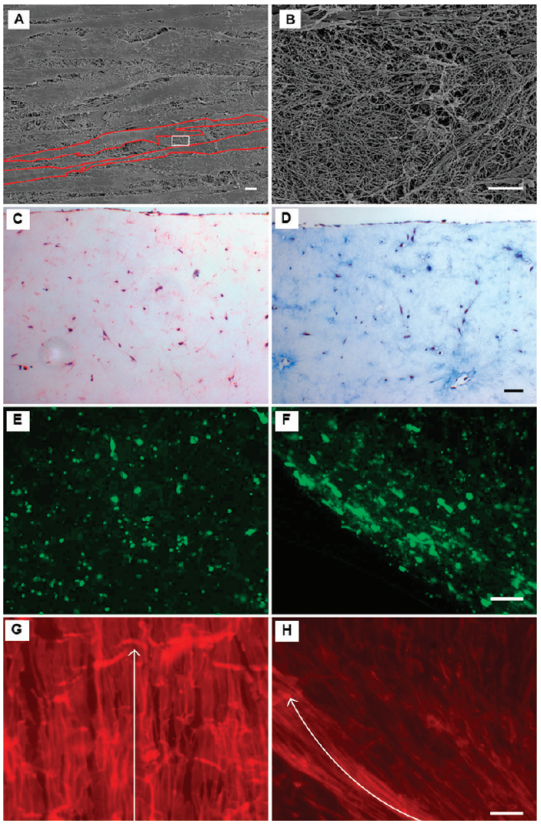

Figure 3. Microscopy gel characterization. SEM images of gel surface structure (A and B, scale bars 5 μm). The SEM images indicate cells growing over the gel surface (A, 1000× magnification) with a magnified area between the cells showing the collagen fiber network in the gel, typically with pores less than 5 μm (B, 3000× magnification). Gel histology cross sections (C and D, scale bar 50 μm) demonstrate uniform cell and collagen distribution throughout the gel. H&E depicts cells as red (C), MSB depicts collagen as blue (D). Viability staining (E and F, scale bar 100 μm) shows viable cells at both the gel center (E) and the gel edge (F) (corresponding dead cell image is available in the Supporting Information, Figure 2). Cellular F-actin immunofluorescence (G and H, scale bar 50 μm) indicates cells at the gel center growing in a parallel direction (G, white arrow denotes cell orientation) and cells at the gel edge growing in line with the contour of the gel (H, white arrow denotes cell orientation). This figure demonstrates that the gel is a good tissue-equivalent model.

tissue penetration, only the 100 nm mNPs were used in all further investigations.

Fluorescence Microscopy. In order to visualize the interaction of 100 nm mNPs with the surface layer of the gel, gels were imaged on a fluorescence microscope after 18 h of incubation with plain or penetratin 100 nm mNPs, ± a MF. Results indicate that a high number of both plain and penetratin mNPs became associated with the surface of the gel in all conditions (Figure 6). From these images it is suggested that without a MF there are more penetratin mNPs on the surface of the gel (Figure 6E) than there are plain mNPs (Figure 6C). This observation was confirmed by analysis in Image J. This reflects the ability of penetratin to enable the mNPs to become cell-associated on the surface of the gel. While this technique was useful to visualise mNP interaction on the gel surface, the depth of gel uptake of 100 nm penetratin mNPs was assessed using confocal microscopy.

Confocal Microscopy. To assess the depth of 100 nm penetratin mNP uptake, gels (with a total depth of 3 mm) were imaged on a confocal microscope, ± a MF, after 1 and 22 h incubation. This allowed visualization of the fluorescent mNPs within the gel through the *z*-axis and consequent measurement of the depth to which they had penetrated ± a MF (Figure 7). The Z-stacks showed that 1 h incubation ± MF and also 22 h incubation − MF resulted in a shallow penetration depth with no significant difference between groups. Thus, 100 nm penetratin mNPs were able to penetrate the gel only to a very minimal depth, which was not increased with longer incubation. However, when a MF was applied, after a 22 h incubation mNP uptake distance was increased on average by 503% ($p < 0.01$), to a depth of 728 μm, at a rate of 33 μm h^{-1}. (Plain 100 nm mNPs exhibited a similar trend, but on a less obvious scale; results not shown here.) This experiment demonstrates that penetratin alone does not facilitate mNP movement in 3D, but if aided by a MF and incubated for enough time, functionalized mNPs can be pulled to a considerable depth within the gel. These results are in agreement with the findings of fluorescence microscopy (Figure 6), which indicate that there is a higher density of penetratin mNPs evident on the gel surface without a MF (Figure 6E) as compared to with a MF (Figure 6F).

Transmission Electron Microscopy (TEM). Confocal results demonstrate that a MF was able to pull mNPs into the gel. However it is important to identify if these functionalized mNPs were being taken up by cells at this depth, a requirement for *in vivo* drug delivery; thus TEM was used to image gels after incubation with 100 nm penetratin mNPs for 18 h, ± a MF (Figure 8). These mNPs were seen within cells at a gel depth of around 500 μm, when treated with a MF (Figure 8A and B). (Plain mNPs were not evident in cells at this depth, thus are not represented.) In contrast, no mNPs were seen at this depth in gels that had not been treated with a MF (for comparison please see Supporting Information, Figure 3, which shows 100 nm penetratin mNPs inside cells grown in 2D monolayer cell culture). This experiment supports the confocal results, demonstrating that a MF is able to pull functionalized mNPs through the gel structure, where they can be taken up by cells growing within it. This cellular uptake is most likely aided by penetratin attachment, since the mNPs observed were not located in cellular vesicles (Figure 8A and B), resulting from the fact that CPPs are reported to facilitate direct translocation across the plasma membrane, thereby avoiding the endolysosomal pathway.[40]

SUMMARY AND DISCUSSION

This study has used fibroblast-seeded collagen gels to investigate whether a MF and NP functionalization

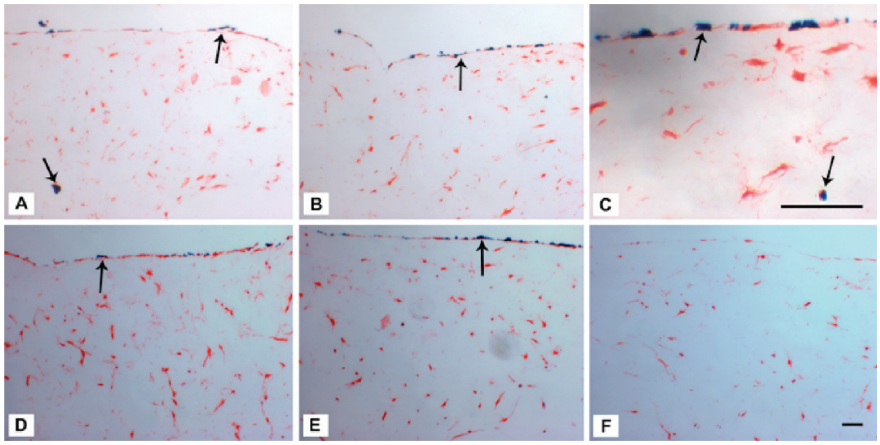

Figure 4. Histology sections of gels stained to visualize iron mNPs. Figure shows gels after incubation with mNPs in a magnetic field (MF) for 18 h, stained with Perls Prussian blue (iron stain). Images refer to 100 nm mNPs (A–C), 200 nm mNPs (D, E), and control sample (F, no mNPs). Plain mNPs are shown in A and D, while penetratin-functionalized mNPs are shown in B and E. Part C refers to penetratin-functionalized 100 nm mNPs at a higher magnification. This figure demonstrates that mNPs became associated with the gel surface (upward-pointing arrows) and were also seen within the gel itself (downward-pointing arrows) [scale bars 50 μm].

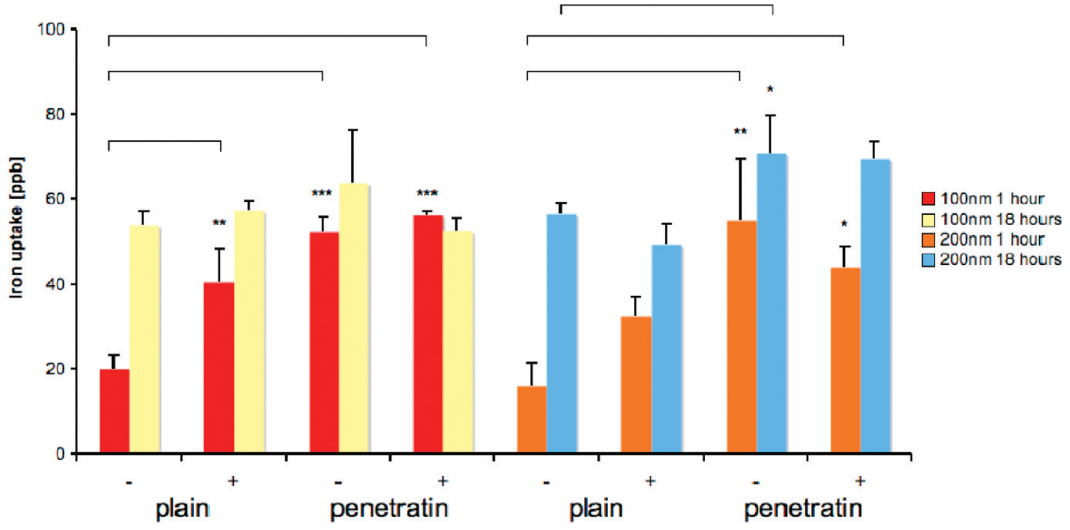

Figure 5. Iron uptake into gels as assessed by ICP-MS. 100 nm mNPs are represented on the left-hand side of this graph by red (1 h) and yellow (18 h) bars. 200 nm mNPs are represented on the right-hand side of this graph by orange (1 h) and blue (18 h) bars. The *x*-axis refers to samples treated without or with a magnetic field (indicated by − or +, respectively), and the staggered *x*-axis labels refer to plain or penetratin-functionalized mNPs. This figure shows that a MF and penetratin both increased the speed of gel–mNP uptake (* = $p < 0.05$, ** = $p < 0.01$, and *** = $p < 0.001$, $n = 3$).

with penetratin can be used to enhance the delivery of mNPs to cells grown in 3D in order to assess the potential of these techniques for *in vivo* drug delivery. To date, several different 3D models have been used to test NP delivery, including acellular gels,[41,42] multicellular spheroids,[43] and multilayer cell cultures.[44] The main shortcomings of such 3D models include an inability to accurately predict cell responses to NPs (acellular gels) and the lack of outside forces such as mechanical stress.[45] Here, results show that cells are evenly distributed throughout the collagen gel (Figure 3C and D), remaining viable at both the gel center and edge (Figure 3E and F), and furthermore, align in a striated fashion (Figure 3A and G), indicative of the inherent cell-mediated gel tensile forces.[46] The characterization results (Figures 2 and 3) suggest that this collagen gel is a realistic tissue-equivalent 3D model suitable for the assessment of NP delivery, overcoming some of the disadvantages associated with previous models.

Gel–mNP uptake analysis showed that on average a MF doubled the speed of gel–mNP uptake (Figure 5) and caused a 5-fold increase in the depth of gel–mNP uptake, occurring at a rate of 33 μm h^{-1} (Figure 7). Penetratin, however, more than doubled the speed of 100 nm gel uptake, more than tripled the speed of 200 nm mNP gel uptake (Figure 5), increased the localization of mNPs to cells on the gel surface (Figure 6), but had no effect on the

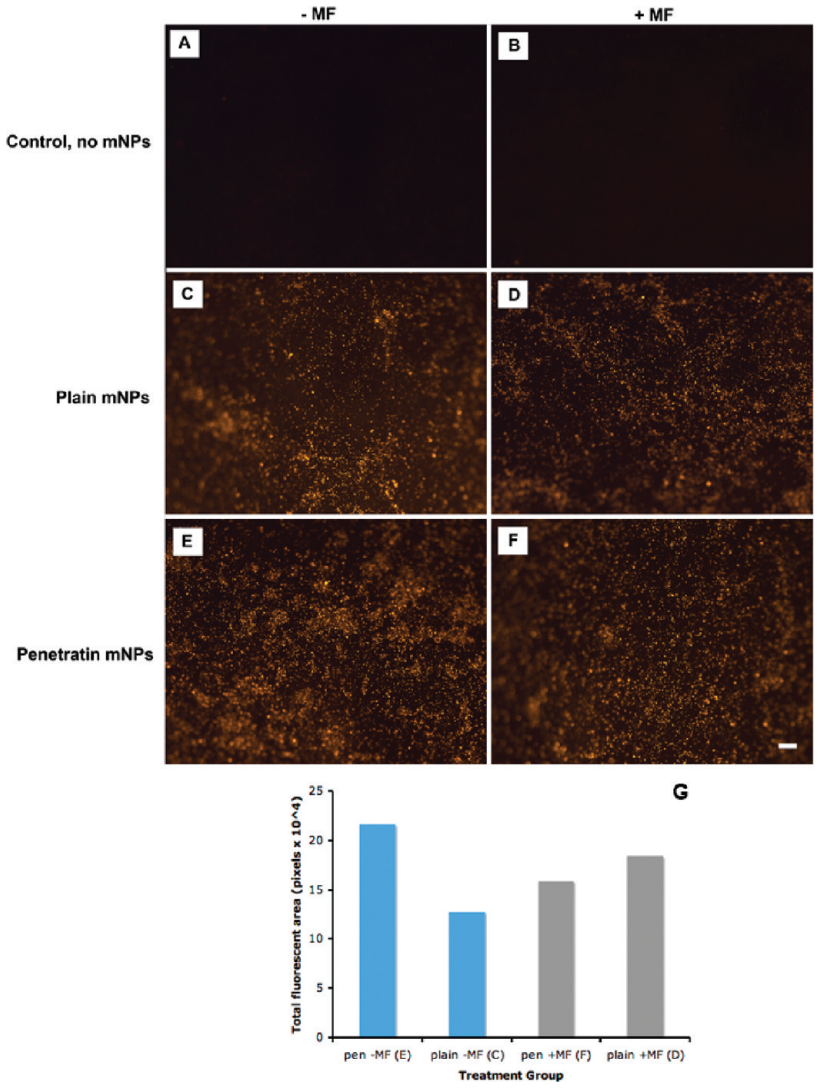

Figure 6. Gel surface localization of 100 nm mNPs after 18 h incubation. Control gels have no mNPs present (A, B). Plain mNPs (C, D) and penetratin mNPs (E, F) are both clearly evident. A, C, and E were incubated without a magnetic field (−MF), whereas B, D, and F were incubated with a magnetic field (+MF). Fluorescent signal was quantified *via* Image J and expressed graphically (G) [scale bar = 50 μm].

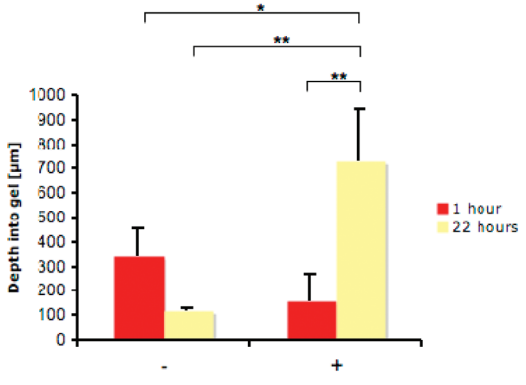

Figure 7. Gel uptake depth of 100 nm penetratin mNPs. On the *x*-axis, samples treated without or with a MF are indicated by − or +, respectively. Red or yellow bars refer to 1 or 22 h of incubation, respectively. The figure indicates that after 22 h a magnetic field has significantly increased the depth of gel uptake of 100 nm penetratin mNPs (* $p < 0.05$, ** $p < 0.01$, $n = 3$).

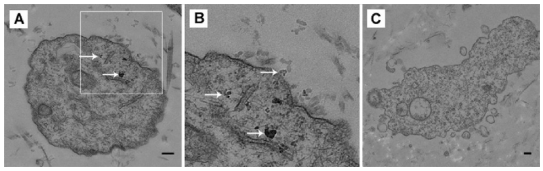

Figure 8. Cellular uptake of 100 nm penetratin mNPs in 3D. (A and B) mNPs (indicated by white arrows) that have been taken up into a cell within a collagen gel in the presence of a magnetic field (MF) at a depth of around 500 μm into the gel. (B) Magnified section of A. (C) Control gel (no mNPs). This figure demonstrates that the combination of a CPP with a MF can facilitate the delivery of mNPs to cells growing in 3D [scale bars = 200 nm]. (A comparison of mNP uptake in 2D monolayer culture is available in the Supporting Information, Figure 3.)

depth of gel−mNP uptake (Figure 7). The trends observed with the ICP-MS data were the same for both 100 and 200 nm mNPs (Figure 5). The only notable difference was that penetratin (−MF) resulted in a greater increase

TABLE 1. Chemical Description of mNPs after Functionalization with Penetratin[a]

	mNPs (mg)	mNPs (nmol)	~molar ratio [mNP:sulfoSMCC]	penetratin added (nmol)	~molar ratio [mNP:added penetratin]
nano-screenMAG/G-PEA (100 nm)	10	30×10^{-3}	[1:38 × 10^3]	29	[1:1 × 10^3]
nano-screenMAG/G-PEA (200 nm)	10	3.7×10^{-3}	[1:310 × 10^3]	29	[1:7.8 × 10^3]

[a] The concentration of mNPs in each 1 mL sample is displayed in both mg and nmol. The molar ratio of mNPs to sulfo-SMCC used for amine activation is shown. The concentration of penetratin in each 1 mL sample and the molar ratio of mNPs to penetratin are also shown.

in the gel uptake of 200 nm mNPs compared with the 100 nm mNPs. This difference could be an artifact, as the 200 nm mNPs have a larger hydrodynamic diameter and they may contain more iron, meaning that even though the level of iron uptake was different, the number of particles taken up may actually be the same. It is likely that the difference in penetratin-induced uptake was caused by the 200 nm mNPs carrying more penetratin molecules per particle than the 100 nm mNPs (Table 1), resulting in increased cell uptake. As smaller NPs were considered to be better drug delivery candidates (due to cell accessability in the tight collagen matrix and their larger surface area to volume ratio), the 100 nm mNPs were used in all further investigations.

It is useful to clarify that "increased speed of uptake" refers to the fact that the level of gel−mNP uptake that occurred under the influence of a MF/penetratin was higher than that of the control mNPs (no MF/penetratin) after 1 h, but became equal to that of the control mNPs after 18 h (Figure 5). We know that the sample did not run out, thereby preventing any further uptake, because the level of uptake reached after 18 h always remained lower than the total level of sample that the gels were challenged with (Supporting Information, Figure 1). Therefore it seems more likely that, for some reason, the gels have a maximum threshold level of gel−mNP uptake, which was reached much faster than normal under the influence of a MF/penetratin, but once reached, it could not be increased any further. This threshold could in part be due to cellular saturation with mNPs, since similar results have been previously described in 2D studies of magnetofection.[17,18]

Effect of the Magnetic Field. MFs are commonly used to pull mNPs into cells grown in 2D. The confocal data demonstrated that MFs are also able to pull mNPs into 3D systems: pulling 100 nm penetratin mNPs to an average depth of 728 μm, at a rate of 33 μm h^{-1} (Figure 7). Similar 3D studies by Kuhn *et al.* have reported that, under the influence of a static MF (100−500 mT), 145 nm mNPs traveled through a hydrogel at 1.5 mm h^{-1} [47] and traveled through a collagen-supplemented gel at 90 μm h^{-1} when functionalized with the enzyme collagenase.[48] Collagen is one of the main components of the ECM,[49] and these comparative studies demonstrate that the presence of this protein significantly increases resistance to mNP movement. This highlights the importance of testing NP delivery in a 3D model that realistically represents the barrier to NP delivery posed by the ECM. Our results demonstrate that a MF causes on average a 5-fold increase in the depth of gel−mNP uptake, and the literature suggests that mNP functionalization with a proteolytic enzyme such as collagenase could increase this depth even further.

Effect of the CPP. It is well reported that CPPs increase cellular uptake of associated NPs in 2D cell systems. In this 3D model system, a cell layer was observed on the gel surface (Figure 3A), most likely due to the initial gel contraction, causing a concentration of cells at the periphery. Penetratin-induced gel−mNP uptake is thus most likely caused by the increased uptake of mNPs into this surface layer of cells. The confocal data confirmed that penetratin mNPs did not move deeply into the gel and away from this surface layer without a MF (Figure 7). This lack of movement is in fact the main problem when trying to target functionalized NPs to a diseased tissue *in vivo*. Therefore it is imperative that CPPs be used in conjunction with a targeting technique, such as a MF, to enable mNPs to reach and subsequently enter target cells, in order to facilitate drug delivery. We demonstrated this combined approach *via* TEM, which showed that following magnetically induced movement through the gel, the 100 nm penetratin mNPs were able to achieve cellular uptake at this increased depth within the gel (Figure 8). Due to the fact that these mNPs were seen free in the cytoplasm, it is likely that they translocated directly across the plasma membrane, facilitated by the attached CPP, thus supporting the hypothesis that CPPs can be used to prevent degradation by the endolysosomal pathway.[40] This work has demonstrated that if used together, a MF and CPPs show huge potential to facilitate targeted drug delivery *in vivo*.

CONCLUSION

This study has been one of the first to investigate the combined effects of a MF and CPPs on the delivery of mNPs to cells growing in a 3D environment. This proof-of-concept study has shown that a MF is able to significantly enhance movement of mNPs through a 3D system, while CPPs are able to enhance the cellular uptake. More importantly, it has

also demonstrated that these techniques can be used in conjunction to magnetically target mNPs functionalized with penetratin deeper into a 3D system. On the basis of these results we predict that the best strategy for site-specific drug delivery *in vivo* will be to use these techniques together, thereby providing both targeting and cellular uptake of drug-loaded mNPs.

EXPERIMENTAL SECTION

NP Functionalization. Iron oxide magnetic green-fluorescence nanoparticles (100 and 200 nm, nano-screenMAG/G-PEA) were bought from Chemicell GmbH (article no. 4417). The amine groups of each mNP sample were activated with sulfosuccinimidyl 4-[*N*-maleimidomethyl]cyclohexane-1-carboxylate (sulfo-SMCC) for further functionalization with the peptide penetratin. The amount of penetratin added aimed to derivatize 1000 of the activated amino groups on the 100 nm mNPs and 7800 on the 200 nm mNPs. This difference was to allow for the difference in surface area between the two sizes of mNPs. Therefore, supposing that the sulfo-SMCC activation and the peptide coupling worked 100%, the mNP to penetratin molar ratio is 1:1000 for the 100 nm size and 1:7800 for the 200 nm size. Both sizes were prepared to a final concentration of 1 mg/mL of mNPs in H_2O.

Reaction Details. To functionalize the 100 nm mNPs, 335 μL from a 30 mg/mL stock solution of 100 nm mNPs was added to 165 μL of freshly prepared ice-cold buffer. To functionalize the 200 nm mNPs, 290 μL from a 35 mg/mL stock solution of 200 nm mNPs was added to 210 μL of freshly prepared ice-cold buffer. Buffer used (100 mM 2-(*N*-morpholino)ethanesulfonic acid, 150 mM NaCl, pH 7.2) contained 500 μg of sulfo-SMCC (article no. 22322 from Pierce). The two reaction mixtures were incubated for 30 min at room temperature, and then 15 μL from a 5 mg/mL solution of activated penetratin 1 (cat. no. PENA0500 from MP Biomedicals) was added to each. The reaction mixtures were incubated overnight at 4 °C. The functionalized nanoparticles were washed by magnetic precipitation with the previously used buffer to remove excess sulfo-SMCC and peptide. Their final volume was adjusted to 1 mL (see Table 1).

NP Characterization. A 2 μL aliquot of each NP solution (0.1 mg/mL in Milli-Q H_2O) was dried onto a carbon-coated grid and viewed under a Leo 912 AB TEM at 120 kV, at 40 000× magnification. Further characterization with regard to sizing *via* dynaminc light scattering and zeta potential is detailed in the Supporting Information, Table 1.

Gel Synthesis. Infinity telomerase-immortalized primary human fibroblasts (h-TERT-BJ1, Clontech Laboratories, Inc.) were grown in T75 flasks in complete medium and passaged by trypsinization when confluent. Cells were cultured at 37 °C with 5% CO_2. The medium used was 71% Dulbecco's modified Eagle's medium (DMEM) (Sigma), 17.5% Medium 199 (Sigma), 10% fetal bovine serum (FBS) (Lonza), 0.5% 100 mM sodium pyruvate (Life Technologies, UK), and 1% penicillin−streptomycin. Gels were made in batches of six by mixing (on ice) 0.5 mL of FBS, 0.5 mL of 10× DMEM, 1 × 10^6 h-TERT cells suspended in 0.5 mL of complete medium, 2.5 mL of Type 1 collagen (First Link UK Ltd.), and 3.5 mL of 0.1 M NaOH (Sigma). The gel mixture was vortexed, pipetted into a 24-well plate (1 mL per well), and incubated at 37 °C overnight to solidify. A needle was run around the edge of each solid gel to detach it from the plastic. Fresh complete media was added and changed weekly. Following diameter measurements, gels were used in experiments four days after detachment to allow full gel contraction.

Gel Characterization. *Rheology.* To verify the mechanical properties of the gels, dynamic frequency sweep experiments were carried out on a strain-controlled rheometer (CSL_{500} Carri-Med rheometer) using a parallel-plate geometry (20 mm diameter). The experiments were performed at 25 °C, and this temperature was controlled throughout the experiment using an integrated electrical heater. Extra precautions were taken to minimize solvent evaporation and to keep the sample hydrated by using a solvent trap and by saturating the internal atmosphere with H_2O. To ensure the measurements were made in the linear viscoelastic region, an amplitude sweep was performed, and the results showed no variation in elastic modulus (G') and viscous modulus (G'') up to a strain of 0.01%. The dynamic modulus of the gel was measured as a frequency function where the frequency sweeps were carried out between 1 and 40 Hz. Measurements were repeated at least three times to ensure reproducibility. Gels were not fixed before use.

Atomic Force Microscopy. AFM analysis was carried out with a NanoWizard II Bio AFM (JPK Instruments, Berlin) mounted on a Zeiss Observer A1 inverted optical microscope. The complete setup was acoustically isolated in order to reduce the interference of ambient noise during the measurements. The probes used for the indentations were prepared in-house by attaching a 4.8 μm silica microsphere (Microparticles Gmbh, Berlin) to a tipless silicon nitride cantilever (Arrow-TL1, NanoWorld) using a UV curable glue (Loctite 349). Before any measurements were recorded the spring constant of the modified cantilever was determined using the thermal calibration method according to the JPK user manual. The value was 0.121 N/m. Force−indentation curves were carried out at 10 μm/s with a 10 μm Z-ramp until a maximum force of 5 nN was reached. Three positions spread evenly across the surface of the gel were selected for indentation measurements. Gels were not fixed before use.

Scanning Electron Microscopy (SEM). Gels were fixed in 1.5% gluteraldehyde in 0.1 M sodium cacodylate (Agar UK) at 4 °C for 1.5 h, then postfixed in 1% osmium tetroxide for 1 h (Agar UK). Samples were subsequently stained with 0.5% uranyl acetate and dehydrated through a series of alcohol increments (30%, 50%, 70%, 90%, 100%, 100% (dry)) and hexamethyl-disilazane (Sigma). After dehydration, gels were then air-dried and viewed on a Jeol 6400 SEM at an accelerating voltage of 6 kV, at 1000× or 3000× magnification.

Histology. Gels were fixed in 4% formaldehyde/phosphate-buffered saline (PBS) with 1% sucrose at 37 °C for 15 min, submerged in 1 mL of permeabilization buffer at 4 °C for 15 min, and embedded in paraffin wax. Sections of 4 μm thickness were cut from the gel center onto polysine-coated slides (CellPath, UK) and baked at 60 °C overnight. Sections were then dewaxed in xylene for 5 min and rehydrated through graded alcohols (100%, 70%) before rinsing with H_2O for 5 min. After rinsing, sections were stained with hematoxylin and eosin (H&E) to display general structures present or Martius scarlet blue (MSB) to display fibrin/connective tissue. After staining, sections were dehydrated through graded alcohols (70%, 100%), placed in xylene for 1 min, and mounted and imaged on a Zeiss Axiovert 25 light microscope at 10× magnification.

Cell Viability. Cell viability was assessed after 96 h using a live/dead staining kit (Invitrogen, UK). Gels were incubated at 37 °C for 1 h in 600 μL of calcein AM and ethidium homodimer (1 μL/ml in DMEM). Images were taken on a Leica Leitz DMRB fluorescence microscope at 10× magnification.

Cell Cytoskeleton F-Actin Immunofluorescence. Gels were fixed as per Section 5.4.4 and then incubated with rhodamine phalloidin (1:50 in PBS/BSA) at 37 °C for 1 h. Gels were rinsed twice with PBS between each step. Images were taken on a Leica Leitz DMRB fluorescence microscope at 20× magnification.

Uptake Analysis. For all uptake experiments, gels were transferred to a 96-well plate and incubated with 75 μL of the mNP solution (0.1 mg/mL in DMEM). Control gels were incubated with 75 μL of DMEM. A static MF was applied by sitting the 96-well plates on top of a MagnetoFACTOR-96 device (Chemicell), which delivered a magnetic force of 280 mT to each well. Gel−mNP incubation was performed in this manner at 37 °C for the time periods indicated in each experiment.

Histology. Gel−mNP incubation was performed with all four mNP species (100 nm plain/penetratin, 200 nm plain/penetratin)

± a MF, for 18 h. Gels were then washed twice in PBS and processed as in Section 5.4.4. Sections were stained with Perls Prussian blue to visualize the mNPs (stains iron) and imaged on a Zeiss Axiovert 25 light microscope at 10× and 40× magnification.

Inductively Coupled Plasma Mass Spectrometry. To quantify mNP uptake into the gels, iron levels in the media were measured by ICP-MS. Gel−mNP incubation was performed with all four mNP species (100 nm plain/penetratin, 200 nm plain/penetratin), ± a MF, for either 1 or 18 h. In an identical manner, each mNP sample was also incubated without a gel for comparison. After incubation, the media from each gel was removed and its remaining iron level was measured by ICP-MS (THERMO X Series II) (Supporting Information, Figure 1). This data were normalized and converted to show the amount of iron that had been taken up into the gel using the following relationship: iron uptake = (iron level after incubation *without* gel) − (iron level after incubation *with* gel). The converted values for iron uptake were averaged (n = 3) and used for statistical analysis and graphical representation (Figure 5).

Fluorescence Microscopy. To assess the surface localization of 100 nm mNPs, gels were incubated with 100 nm plain/penetratin mNPs, ± a MF, for 18 h. Gels were then washed twice in PBS. Images of the gels' top surfaces were taken on a Zeiss Axiophot fluorescence microscope at 10× magnification.

Confocal Microscopy. To assess the depth of 100 nm penetratin mNP uptake, gels were incubated with 100 nm penetratin mNPs, ± a MF, for 1 or 22 h. After incubation, gels were washed twice in PBS and fixed in 4% formaldehyde/PBS with 1% sucrose for 25 min. A Zeiss LSM 510 META confocal microscope (at 10× magnification) was then used to produce a z-stack of each gel composed of sequential images taken 1 μm apart. Each compressed z-stack was analyzed from the first image downward through the gel, and the depth of mNP penetration was recorded. These distances were then averaged (n = 3) and used for statistical analysis and graphical representation (Figure 7).

Transmission Electron Microscopy. To visualize the cellular interaction of 100 nm penetratin mNPs, gels were incubated with 100 nm penetratin mNPs, ± a MF, for 18 h. Gels were cut into quarters and fixed as per Section 5.4.3. Samples were postfixed in 1% osmium tetroxide in phosphate buffer for 1 h followed by 0.5% uranyl acetate for 1 h and then taken through alcohol dehydration increments and left in propylene oxide Epon 812 resin mix (1:1) overnight. Gels were put into pure resin and keep in an oven for 24 h to cure. Blocks were then cut into ultrathin sections, stained with 2% methanolic uranyl acetate and Reynolds lead citrate, and viewed under a Leo 912 AB TEM at 120 kV.

Statistics. Statistical analysis was performed in SPSS. The ICP-MS data for each size of mNP (100 or 200 nm) for each time point (1 or 18 h) were analyzed by one-way ANOVA with Dunnett's test. The confocal data were analyzed by one-way ANOVA with Tukey's test. For the rheology, ICP-MS, and confocal data, n = 3. In all figures * = $p < 0.05$, ** = $p < 0.01$, and *** = $p < 0.001$.

Acknowledgment. We thank the Royal Society and the European Commission (Nanosci Eplus) for funding of the work described in this paper.

Supporting Information Available: This material is available free of charge *via* the Internet at http://pubs.acs.org.

REFERENCES AND NOTES

1. Sawant, R.; Torchilin, V. Intracellular Transduction Using Cell-Penetrating Peptides. *Mol. Biosyst.* **2010**, *6*, 628–640.
2. Parveen, S.; Sahoo, S. K. Polymeric Nanoparticles for Cancer Therapy. *J. Drug Targeting* **2008**, *16*, 108–123.
3. Ahmad, M. Z.; Akhter, S; Jain, G. K.; Rahman, M; Pathan, S. A.; Ahmad, F. J.; Khar, R. K. Metallic Nanoparticles: Technology Overview & Drug Delivery Applications in Oncology. *Expert Opin. Drug Delivery* **2010**, *7*, 927–942.
4. Berry, C. C. Curtis ASG. Functionalisation of Magnetic Nanoparticles for Applications in Biomedicine. *J. Phys. D−Appl. Phys.* **2003**, *36*, R198–R206.
5. Dobson, J. Gene Therapy Progress and Prospects: Magnetic Nanoparticle-Based Gene Delivery. *Gene Ther.* **2006**, 283–287.
6. Widder, K. J.; Senyei, A. E.; Scarpelli, D. G. Magnetic Microspheres - Model System for Site Specific Drug Delivery *in Vivo*. *Proc. Soc. Exp. Biol. Med.* **1978**, *158*, 141–146.
7. Jain, T. K.; Reddy, M. K.; Morales, M. A.; Leslie-Pelecky, D. L.; Labhasetwar, V. Biodistribution, Clearance, and Biocompatibility of Iron Oxide Magnetic Nanoparticles in Rats. *Mol. Pharm.* **2008**, *5*, 316–327.
8. Lubbe, A. S.; Bergemann, C.; Huhnt, W.; Fricke, T.; Riess, H.; Brock, J. W.; Huhn, D. Preclinical Experiences with Magnetic Drug Targeting: Tolerance and Efficacy. *Cancer Res.* **1996**, *56*, 4694–4701.
9. Jaganathan, H; Ivanisevic, A. *In Vitro* Cytotoxic Evaluation of Metallic and Magnetic DNA-Templated Nanostructures. *ACS Appl. Mater. Interfaces* **2010**, *2*, 1407–1413.
10. Corchero, J. L.; Villaverde, A. Biomedical Applications of Distally Controlled Magnetic Nanoparticles. *Trends Biotechnol.* **2009**, *27*, 468–476.
11. Wu, S. Y.; Zhang, L. J.; Zhong, J. H.; Zhang, Z. L. Dual Contrast Magnetic Respnance Imaging Tracking of Iron-Labeled Cells in Vivo. *Cytotherapy* **2010**, *12*, 859–869.
12. Laurent, S.; Boutry, S.; Mahieu, I.; Vander Elst, L.; Muller, R. N. Iron Oxide Based MR Contrast Agents: From Chemistry to Cell Labeling. *Curr. Med. Chem.* **2009**, *16*, 4712–4727.
13. Dobson, J. Gene Therapy Progress and Prospects: Magnetic Nanoparticle-Based Gene Delivery. *Gene Ther.* **2006**, *13*, 283–287.
14. Pickard, M.; Chari, D. Enhancement of Magnetic Nanoparticle-Mediated Gene Transfer to Astrocytes by 'Magnetofection': Effects of Static and Oscillating Fields. *Nanomedicine* **2010**, *5*, 217–232.
15. Mah C, Zolotukhin I, Fraites T. J., Dobson J, Batich C, Byrne B. J. Microsphere-Mediated Delivery of Recombinant AAV Vectors *in Vitro* and *in Vivo*. *Mol. Ther.* **2000**, *1*.
16. Mah, C; Fraites, T. J.; Zolotukhin, I; Song, S. H.; Flotte, T. R.; Dobson, J; Batich, C; Byrne, B. J. Improved Method of Recombinant AAV2 Delivery for Systemic Targeted Gene Therapy. *Mol. Ther.* **2002**, *6*, 106–112.
17. Plank, C.; Scherer, F.; Schillinger, U.; Bergemann, C.; Anton, M. Magnetofection: Enhancing and Targeting Gene Delivery with Superparamagnetic Nanoparticles and Magnetic Fields. *J. Lipid Res.* **2003**, *13*, 29–32.
18. Plank, C.; Schillinger, U.; Scherer, F.; Bergemann, C.; Remy, J. S.; Krotz, F.; Anton, M.; Lausier, J.; Rosenecker, J. The Magnetofection Method: Using Magnetic Force to Enhance Gene Delivery. *Biol. Chem.* **2003**, *384*, 737–747.
19. Berry, C. C. Intracellular Delivery of Nanopartides *via* the HIV-1 Tat Pepticle. *Nanomedicine* **2008**, *3*, 357–365.
20. Schwarze, S. R.; Dowdy, S. F. In Vivo Protein Transduction: Intracellular Delivery of Biologically Active Proteins, Compounds and DNA. *Trends Pharmacol. Sci.* **2000**, *21*, 45–48.
21. Derossi, D.; Joliot, A. H.; Chassaing, G.; Prochiantz, A. The 3rd Helix of the Antennapedia Homodomain Translocates through Biological-Membranes. *J. Biol. Chem.* **1994**, *269*, 10444–10450.
22. Josephson, L.; Tung, C. H.; Moore, A.; Weissleder, R. High-Efficiency Intracellular Magnetic Labeling with Novel Superparamagnetic-Tat Peptide Conjugates. *Bioconjugate Chem.* **1999**, *10*, 186–191.
23. Smith, C.-A.; de la Fuente, J.; Pelaz, B.; Furlani, E. P.; Mullin, M.; Berry, C. C. The Effect of Static Magnetic Fields and Tat Peptides on Cellular and Nuclear Uptake of Magnetic Nanoparticles. *Biomaterials* **2010**, *31*, 4392–4400.
24. Sawant, R. M.; Hurley, J. P.; Salmaso, S.; Kale, A.; Tolcheva, E.; Levchenko, T. S.; Torchillin, V. P. "SMART" Drug Delivery Systems: Double-Targeted pH-Responsive Pharmaceutical Nanocarriers. *Bioconjugate Chem.* **2006**, *17*, 943–949.
25. de la Fuente, J. M.; Berry, C. C. Tat Peptide As an Efficient Molecule to Translocate Gold Nanoparticles into the Cell Nucleus. *Bioconjugate Chem.* **2005**, *16*, 1176–1180.
26. Garden, O. A.; Reynolds, P. R.; Yates, J.; Larkman, D. J.; Marelli-Berg, F. M.; Haskard, D. O.; *et al*. A Rapid Method for Labelling CD4(+) T Cells with Ultrasmall Paramagnetic Iron Oxide Nanoparticles for Magnetic Resonance Imaging That Preserves Proliferative, Regulatory and Migratory Behaviour *in Vitro*. *J. Immunol. Methods* **2006**, *314*, 123–133.

27. Berry, C. C.; Harianawalw, H.; Loebus, J.; Oreffo, R. O. C.; de la Fuente, J. Enhancement of Human Bone Marrow Cell Uptake of Quantum Dots Using Tat Peptide. *Curr. Nanosci.* **2009**, *5*, 390–395.
28. Lindgren, M.; Hallbrink, M.; Prochiantz, A.; Langel, U. Cell-Penetrating Peptides. *Trends Pharmacol. Sci.* **2000**, *21*, 99–103.
29. Mukherjee, S.; Ghosh, R. N.; Maxfield, F. R. Endocytosis. *Physiol. Rev.* **1997**, *77*, 759–803.
30. Deshayes, S.; Morris, M. C.; Divita, G.; Heitz, F. Cell-Penetrating Peptides: Tools for Intracellular Delivery of Therapeutics. *Cell. Mol. Life Sci.* **2005**, *62*, 1839–1849.
31. Bell, E.; Ivarsson, B.; Merrill, C. Production of a Tissue-Like Structure by Contraction of Collagen Lattices by Human-Firbroblasts of Different Proliferative Potential *in Vitro*. *Proc. Natl. Acad. Sci. U. S. A.* **1979**, *76*, 1274–1278.
32. Berry, C. C.; Shelton, J. C.; Lee, D. A. Cell-Generated Forces Influence the Viability, Metabolism and Mechanical Properties of Fibroblast-Seeded Collagen Gel Constructs. *J. Tissue Eng. Regen. Med.* **2009**, *3*, 43–53.
33. Zhang, H. Y.; Lee, M. Y.; Hogg, M. G.; Dordick, J. S.; Sharfstein, S. T. Gene Delivery in Three-Dimensional Cell Cultures by Superparamagnetic Nanoparticles. *ACS Nano* **2010**, *4*, 4733–4743.
34. Abbott, A. Cell Culture: Biology's New Dimension. *Nature* **2003**, *424*, 870–872.
35. Cheng, K.; Lai, Y. Z.; Kisaalita, W. S. Three-Dimensional Polymer Scaffolds for High Throughput Cell-Based Assay Systems. *Biomaterials* **2008**, *29*, 2802–2812.
36. Sivaraman, A.; Leach, J. K.; Townsend, S.; Iida, T.; Hogan, B. J.; Stolz, D. B.; Fry, R.; Samson, L. D.; Tannenbaum, S. R.; Griffith, L. G. A Microscale *in Vitro* Physiological Model of the Liver: Predictive Screens for Drug Metabolism and Enzyme Induction. *Curr. Drug Metab.* **2005**, *6*, 569–591.
37. Yamada, K. M.; Clark, K. Cell Biology - Survival in Three Dimensions. *Nature* **2002**, *419*, 790–791.
38. Alonso, J. L.; Goldmann, W. H. Feeling the Forces: Atomic Force Microscopy in Cell Biology. *Life Sci.* **2003**, *72*, 2553–2560.
39. Discher, D. E.; Mooney, D. J.; Zandstra, P. W. Growth Factors, Matrices, and Forces Combine and Control Stem Cells. *Science* **2009**, *324*, 1673–1677.
40. Jarver, P.; Langel, U. Cell-Penetrating Peptides - A Brief Introduction. *Biochim. Biophys. Acta, Biomembr.* **2006**, *1758*, 260–263.
41. Kim, Y.; Dalhaimer, P.; Christian, D. A.; Discher, D. E. Polymeric Worm Micelles As Nano-Carriers for Drug Delivery. *Nanotechnology* **2005**, *16*, S484–S491.
42. Valentine, M. T.; Perlman, Z. E.; Gardel, M. L.; Shin, J. H.; Matsudaira, P.; Mitchison, T. J.; Weitz, D. A. Colloid Surface Chemistry Critically Affects Multiple Particle Tracking Measurements of Biomaterials. *Biophys. J.* **2004**, *86*, 4004–4014.
43. Goodman, T. T.; Olive, P. L.; Pun, S. H. Increased Nanoparticle Penetration in Collagenase-Treated Multicellullar Spheroids. *Int. J. Nanomed.* **2007**, *2*, 265–274.
44. Padron, J. M.; van der Wilt, C. L.; Smid, K.; Smitskamp-Wilms, E.; Backus, H. H. J.; Pizao, P. E.; Giaccone, G.; Peters, G. J. The Multilayered Postconfluent Cell Culture As a Model for Drug Screening. *Crit. Rev. Oncol. Hematol.* **2000**, *36*, 141–157.
45. Goodman, T. T.; Ng, C. P.; Pun, S. H. 3-D Tissue Culture Systems for the Evaluation and Optimization of Nanoparticle-Based Drug Carriers. *Bioconjugate Chem.* **2008**, *19*, 1951–1959.
46. Eastwood, M.; Mudera, V. C.; McGrouther, D. A.; Brown, R. A. Effect of Precise Mechanical Loading on Fibroblast Populated Collagen Lattices: Morphological Changes. *Cell Motil. Cytoskeleton* **1998**, *40*, 13–21.
47. Kuhn, S. J.; Hallahan, D. E.; Giorgio, T. D. Characterization of Superparamagnetic Nanoparticle Interactions with Extracellular Matrix in an *in Vitro* System. *Ann. Biomed. Eng.* **2006**, *34*, 51–58.
48. Kuhn, S. J.; Finch, S. K.; Hallahan, D. E.; Giorgio, T. D. Proteolytic Surface Functionalization Enhances *in Vitro* Magnetic Nanoparticle Mobility through Extracellular Matrix. *Nano Lett* **2006**, *6*, 306–312.
49. Di Lullo, G. A.; Sweeney, S. M.; Korkko, J.; Ala-Kokko, L.; San Antonio, J. D. Mapping the Ligand-Binding Sites and Disease-Associated Mutations on the Most Abundant Protein in the Human, Type I Collagen. *J. Biol. Chem.* **2002**, *277*, 4223–4231.